Automating Event-detection of Brain Neuron Synaptic Activity and Action Potential Firing *in vivo* using a Random-access Multiphoton Laser Scanning Microscope for Real-time Analysis

Kelly D. R. Sakaki, *Member*, *IEEE*, Patrick Coleman *Student Member*, *IEEE*, Tristan Dellazizzo Toth *Student Member*, *IEEE*, Claire Guerrier and Kurt Haas

Abstract—**Determining how a neuron computes requires an understanding of the complex spatiotemporal relationship between its input (e.g. synaptic input as a result of external stimuli) and action potential output. Recent advances in *in vivo,* laser-scanning multiphoton technology, known as random-access microscopy (RAM), can capture this relationship by imaging fluorescent light, emitted from calcium-sensitive biosensors responding to synaptic and action potential firing in a neuron's full dendritic arbor and cell body. Ideally, a continuous output of fluorescent intensities from the neuron would be converted to a binary output ('event', 'or no-event'). These binary events can be used to correlate temporal and spatial associations between the input and output. However, neurons contain hundreds-to-thousands of synapses on the dendritic arbors generating an enormous quantity of data composed of physiological signals, which vary greatly in shape and size. Thus, automating data-processing tasks is essential to support high-throughput analysis for real-time/post-processing operations and to improve operators' comprehension of the data used to decipher neuron computations. Here, we describe an automated software algorithm to detect brain neuron events in real-time using an acousto-optic, multiphoton, laser scanning RAM developed in our laboratory. The fluorescent light intensities, from a genetically encoded, calcium biosensor (GCAMP6m), are measured by our RAM system and are input to our 'event-detector', which converts them to a binary output meant for real-time applications. We evaluate three algorithms for this purpose: exponentially weighted moving average, cumulative sum, and template matching; present each algorithm's performance; and discuss user-feasibility of each. We validated our system *in vivo*, using the visual circuit of the *Xenopus laevis*.**

I. INTRODUCTION

Elaborate dendritic arbors of brain neurons receive hundreds to thousands of synaptic inputs from upstream neurons. This input activity is integrated and processed within the dendritic arbor and cell body, where the output signal is encoded in rates of all-or-none action potential (AP) firing. APs then propagate throughout the axonal arbor to transmit output signals to downstream postsynaptic targets. It remains unknown how the structure and electrophysical properties of dendritic arbors and the positions of synapses across the arbor influence the integration of synaptic information and its transformation into encoded patterns of AP firing output.

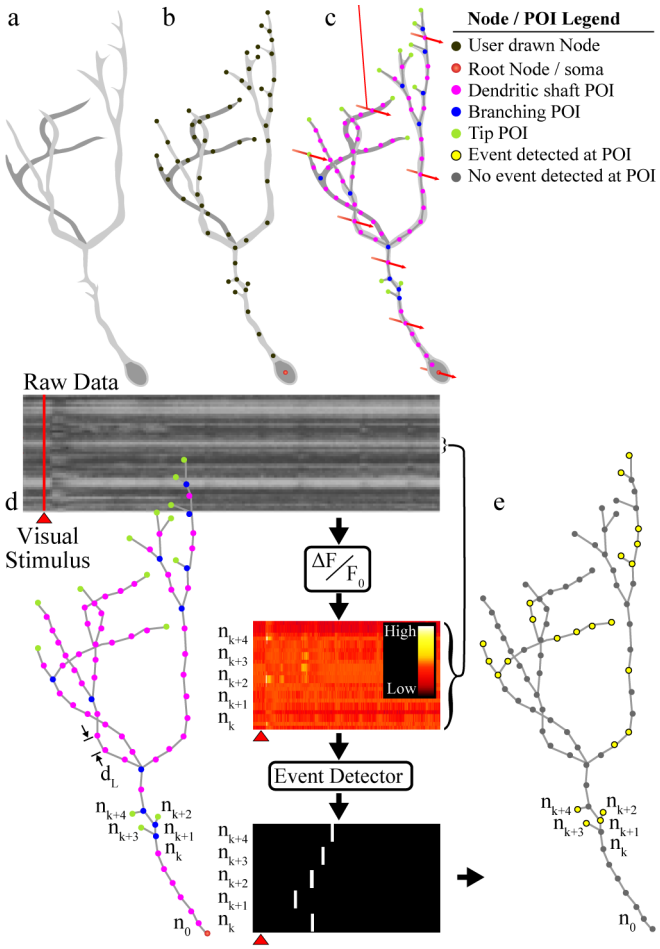

Fig. 1 Event detection in brain neurons. (a) Neurons, expressing a calcium biosensor are localized in the *Xenopus laevis* optic tectum using a multiphoton, laser-scanning, random-access microscope. (b) A 3D-stack of X-Y images allows the operator to trace the neuron's dendritic arbor and cell body, resulting in a 3D skeletonized frame. (c) The frame is automatically refined by converting the frame to points-of-interest (POI) with 2.5 μm spacing along the arbor. The system then scans each POI at calcium imaging rates while visual stimuli are presented and the (d) fluorescent intensities of each POI are recorded as grayscale intensities (i.e. traces). (e) POI traces are converted to $\Delta F/F0$ and sent to an event detector producing an 'event' or 'no-event' output indicating which POIs exhibit activity. The resulting spatiotemporal, binary output can then assist in determining how a neuron integrates synaptic input producing action potential firing output.

This work was supported by the Canadian Institute for Health Research. K. Sakaki, T. Dellazizzo Toth, P. Coleman and K. Haas (Principal Investigator) are with Dept. of Cellular and Physiological Sciences, Faculty of Medicine, Djavad Mowafaghian Centre for Brain Health, University of British Columbia, Vancouver, BC V6T 2B5, Canada. C. Guerrier is with Dept. of Mathematics, Faculty of Science and the Dept. of Cellular and Physiological Sciences. University of British Columbia, Vancouver, BC V6T 1Z2, Canada, and C. Guerrier is partly funded by the Fyssen foundation. (Correspondence e-mail: kelly.sakaki@ubc.ca, P. +1.604.827.5840, F. +1.604.822.7299).

Because both synaptic events and neural encoding properties are highly stochastic, to fully understand synaptic integration, information transformation and neural encoding of APs, it is necessary to record patterns of all neural input and output simultaneously over long periods.

Fully capturing the input/output activity of individual neurons in order to resolve fundamental operations of discrete state-transitions is called 'comprehensive imaging'. Comprehensive imaging requires continuous and simultaneous tracking in real-time of: 1) a neuron's entire dendritic arbor morphology; 2) dendritic arbor activity driven by synaptic input; and 3) AP firing output sampled at the cell body or axon. Neuron *morphology* in an awake and intact brain can be imaged using fluorescent microscopy by labeling individual neurons with a space-filling fluorophore. Since synaptic transmission and AP firing elicit discrete calcium transients, neural *activity* can be detected using fluorescent calcium sensors. Neurons can be filled with calcium-sensitive dyes or transfected for expression of genetically-encoded calcium indicator (GECI) [1], [2] proteins (e.g., GCaMP6 [3]) which respond to fluctuations in intracellular free calcium with changes in their fluorescent properties [4].

Recent advances in deep tissue, multiphoton laser scanning microscope (MPLSM) technologies, known as 'random-access' microscopy [5]–[8], can be exploited for comprehensive imaging by analyzing neurons in the intact and awake brain. 'Random-access' microscopy (RAM) refers to imaging techniques allowing discrete, point-of-interest (POI) sampling by scanning POIs in 2D or 3D without scanning the intervening space between them. While contemporary laser-scanning microscopy captures neuronal morphology by fully imaging the volume encompassing the neuron, RAM POI sampling significantly increases imaging speeds by restricting sampling to the neuronal structure and avoiding the large extracellular tissue. Our recent design of a random-access MLSM [8] can position the laser focal point arbitrarily on a POI in 3D space. Our system can sample at a maximum rate of 23,364 POIs-per-second, and an overall scanning rate of the neuron between 5 and 20 Hz depending on the size and complexity of the arbor. Our system employs a hybrid acousto-optic/piezoelectric actuator, multiphoton laser scanning system. Acousto-optics are inertia-free laser deflectors and offer unprecedented scanning rates [9].

One of the most critical functions of systems with comprehensive imaging capabilities is to be able to convert POI imaging output to meaningful, physiological state representations of the neuron and detect discrete calcium events to facilitate the understanding of how neurons perform dendritic integration (Fig. 1). In terms of data processing functions, this means the system should convert raw, fluorescent calcium biosensor intensities to continuous signals (e.g, calcium transients representing activity), identify and indicate the occurrence of physiological events in the continuous signal and then relate these events to the firing output of the neuron. An inherent challenge to comprehensive imaging, however, is the high rate and large volume of raw data that is generated. The number of POIs recorded for comprehensive imaging of one neuron can range from hundreds to thousands, multiplied by imaging rates exceeding 5 Hz for the entire dendritic arbor. Therefore, manually processing and correlating the spatiotemporal relationships of the calcium transient signals strictly through visual observation is not practical. Thus, there is a great need to automate the processes for converting POI's data to spatiotemporal calcium transients, and to rapidly detect events that represent synaptic and AP activity. Synaptic input and AP output can then be analyzed to decipher information processing and encoding.

In this conference paper, we present the design of an event detector that can be used in real-time detection of synaptic input and AP output from fluorescent calcium signals in neurons *in vivo,* and report tests on candidate algorithms. Given the variances between RAM systems (e.g., noise, performance requirements, etc.) we provide a rigorous and intuitive method for evaluating the performance of different candidate algorithms to be used for event detection.

We implemented and evaluated the performance of three algorithms to be used as event detectors; these include the Exponentially Weighted Moving Average (EWMA); the Cumulative Sum (known as 'cusum') and the Matched Filter (MF). Several characteristics of each algorithm are evaluated, including: accuracy in detecting events, timing considerations and the complexity of use using generated data. We then provide a demonstration, conducted in real-time, of the performance of each algorithm while recording data from a neuron in the awake brain of the *Xenopus laevis*.

II. Methodology

A. Considerations for temporal sampling of neural activity

Brain neurons exhibit both spontaneous and sensory stimulus-evoked synaptic and AP activity. Presenting controlled visual stimuli allows linking evoked activity to information transmission and processing. Synaptic and AP activity can be imaged by analyzing spatiotemporal changes in intracellular free calcium (reviewed in [4], [10]) using calcium-sensitive fluorescent dyes or GECIs [1], [2], such as GCaMP6 [3]. Postsynaptic changes to calcium, during an evoked response, arise from activation of calcium-permeable glutamatergic N-Methyl-D-aspartate (NMDA) [4], [11] and GluA2 subunit-lacking, α-amino-3-hydroxy-5-methyl-4-isoxazolepropionic acid (AMPA) subtypes of glutamate receptors [12].

In neurons, resting cytoplasmic calcium levels are generally quite low, only ~100 nM [13]. As a result, when there is a shift in the conformation of the plasma membrane calcium channels to an open state, there is a rapid influx of calcium (150-300 nM) followed by a fast decay (<100 nM) [14], as measured using electrophysiology instrumentation (i.e. sharp electrode). In neurons expressing GCaMP6, these activity-induced calcium transients can be detected by recording the change in fluorescence intensity which occurs when free intracellular calcium ions bind to the modified calmodulin domain of the GCaMP6 protein, causing a conformational change resulting in increased fluorescence [2]. The synaptic and AP induced fluorescence changes of such calcium biosensors occur on the order of milliseconds (rise time) [15] to seconds (decay time) [16].

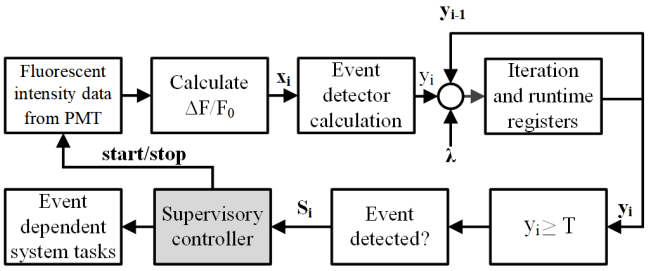

Fig. 2 The event detector, system feedback loop.

Several factors contribute to calcium transients varying in amplitude and rise/decay time, eliminating simple static threshold level detectors, which would otherwise respond incorrectly or fail to respond at all, reducing the accuracy of the system. Consequently, the signal characteristics of the multiphoton-imaged calcium transients warrant special implementation considerations for automated event detection systems. Firstly, because the amplitude of transients is dependent on voltage-gated calcium channels, the amplitude varies due to the degree of calcium influx from different synaptic inputs, which are graded in nature, and the variable number of APs clustered in trains. Secondly, calcium transients possess long decay times, much longer than the duration of the underlying change in membrane potential due to the buffering characteristics of the calcium sensors. Calcium buffering causes a broad dampening effect on the signal output rather than a series of sharp, discrete spikes [14]. Thirdly, inconsistencies in concentration levels [3], [14], and distribution of voltage gated calcium channels [17] will also affect the shape of transients.

B. Selecting candidate event detector algorithms

We identified characteristics to compare between candidate event detectors in order to determine the most suitable one for our system. These included: **1) *Accuracy*** - the system should be robust, not respond to spurious signals (i.e. false-positives, FP), and conversely not miss identifying an event when it does occur (i.e. false-negatives, FN). **2) *Computationally efficient*** – we desire the routine to operate in real-time in order to assess the integration of the neuron. This allows the system to quickly tune stimuli during an experiment in order to evoke the desired response characteristics. Therefore, the event detector should consume as little time as needed in order to determine an event as required. Thus, the event detector algorithm's timing characteristics will be reported. **3) *Intuitive parameters and easy implementation*** - setting parameters, by operators, can be daunting especially when system-characteristics may vary. The number of parameters should be minimized and setting parameter values should be relatively intuitive, and/or provide tools to determine what parameter values would be best in the system. Thus, we describe what the parameters are, provide some tools to determine what settings should be set to and provide some feedback to the reader of the complexity the operator faces in using each event detector.

C. Candidate event detector algorithms

We considered three event detection algorithms including the EWMA, cusum and MF. The event detection module, exists in the main feedback loop (Fig. 2) of the RAM system after the calculation of $\Delta F/F_0$, $(x_i)_i$ (see [18] for the calculation of $\Delta F/F_0$ fluorescent calcium intensities), which are input to the event detector. At each step i, the algorithm computes the statistic, y_i, from the previous observations $(x_k)_{k\leq i}$ and statistic y_{i-1}, through a function:

$$f(x_1, \ldots, x_i, y_{i-1}) \rightarrow y_i \quad (1)$$

Given a threshold T, and the statistic y_i, an event is considered detected whenever y_i crosses the threshold T: $y_i \geq T$ and $y_{i-1} < T$.

1) Exponentially Weighted Moving Average (EWMA)

The EWMA is a moving average that used to detect slow, increasing changes, while avoiding false event detections due to spurious noise. The EWMA is a recursive statistic calculated as follows:

$$y_i = \lambda_e x_i + (1 - \lambda_e) y_{i-1} \quad (2)$$

Equation (2) is the weighted sum of the sample value x_i and the average from previous iteration, y_{i-1}. The only parameter in the EWMA is the 'weight', λ_e, which determines how much the most recent sample should modify the existing average. The values of λ_e range from (0, 1], where values of λ_e approaching 1 will cause y_i to be more jagged and reach T faster, and values of λ_e approaching zero will smooth y_i and be more robust against spurious noise. Some guidance for (2) is provided for choosing suitable thresholds [6]:

$$T = 3\sqrt{\frac{\lambda_e}{2-\lambda_e}} \quad (3)$$

2) Cumulative Sum (i.e. cusum)

The cusum is commonly used in statistical process control applications [19]–[23]. It computes the accumulation of residuals, y_i, or in other words, the growing sum of differences between the current sample x_i, the mean over all the previous samples μ, and λ_s, the 'slack' variable:

$$y_i = max\left(0, y_{i-1} + (x_i - \mu - \lambda_s)\right) \quad (4)$$

Like the EWMA, the cusum is also a recursive statistic. This measures how far above the expected value in an event-free signal each sample is. If the value of λ_s is set to the average absolute value of the noise in the system, x_i that are less-than-or-equal to the average noise value of the system will not increase y_i towards the threshold T. Therefore, y_i will only increase if the value of x_i exceeds the average noise of the system. The sensitivity of the selection of λ_s can vary the results of the system so some caution should be used in selecting this value. As the value of λ_s increases, the cusum becomes more robust to noise with fewer FPs; however, it requires a greater number of samples, x_i, before the threshold is reached resulting in a greater latency before the event is 'known' to be detected (i.e. FN).

3) Matched Filter (MF)

The MF, unlike the EWMA and the cusum, detects events using *a priori* information of the shape of the transient. The MF compares the hypothesis that recent samples come from a transient shape, m, as opposed to that from pure noise [24], [25]. The MF applies a likelihood ratio test to x_i:

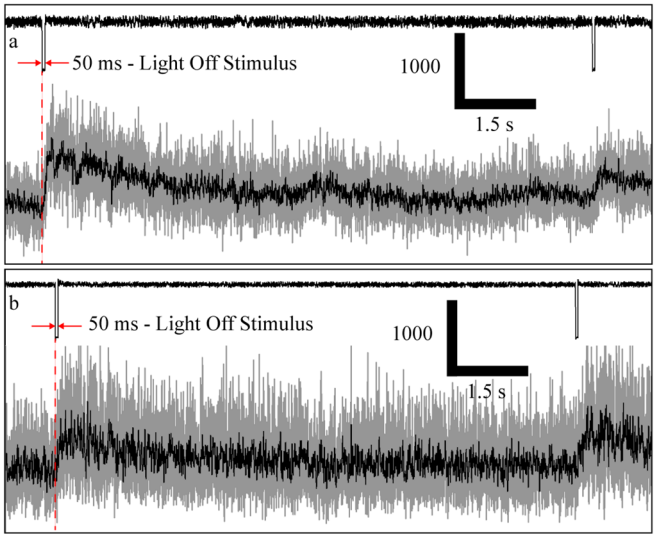

Fig. 3 Evoked, calcium transients. Examples of calcium transients (GCaMP6m) recorded on a MPLSM. Signals are recorded from the (a) cell body and (b) a distil POI on the dendritic arbor.

$$y_i = \sum_{j=1}^{N} log\left(\frac{pdf_n(x_{i-j} - m_{N-j+1})}{pdf_n(x_{i-j})}\right) \quad (5)$$

Here pdf_n represents the noise distribution, and is computed assuming a Gaussian noise distribution [26] where the mean and standard deviation parameters are the average and standard deviation over all previous x_j. The transient signal, m_{N-j+1}, is defined as:

$$m_t = A\frac{\tau_A^{\tau_A/(\tau_A-\tau_B)}\tau_B^{\tau_B/(\tau_B-\tau_A)}}{\tau_B - \tau_A}\left(e^{-t/\tau_B} - e^{-t/\tau_A}\right) \quad (6)$$

with τ_A, the rise time-constant, τ_B the decay time-constant, $\tau_A \leq \tau_B$, and A the peak amplitude of the transient. The template signal was set to match single-exponential rise and decay times as observed in [3]. The values for τ_A = 28 ms and τ_B = 390 ms for GCaMP6m are extracted from [3], and A = 2 was chosen based on our experiments.

The implementation of the MF requires four parameters: the size of the sliding window N, as well three (τ_A, τ_B and A) to characterize the template signal in (6). Higher values of N will increase the accuracy by providing a longer list of samples, $x_{i-N-1}\ldots x_i$, to compare with the template signal. The caveats being that it increases the number of calculations, which increases the latency before an event is detected as well as the computation time. In this algorithm, y_i represents the log of the probability that the last N samples match the template signal m_t, compared to pure noise. The ideal threshold is T = 0, equivalent to performing a likelihood ratio test, identifying when the input is more likely to be from a transient shape. Increasing T will improve precision at the cost of worse recall - the opposite is true for reducing T.

D. *Offline event detector validation*

The three candidate event detectors were initially tested by generating simulated, raw calcium intensities, which allowed us to compare the output of the event detectors with the actual location of the simulated event (i.e. calcium transient). 100 simulated, pseudorandom transients (Fig. 4a) were separated by 8-12 seconds at a sampling rate of 10 Hz.

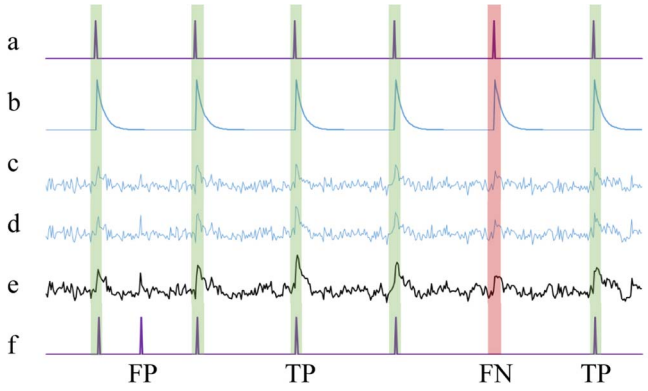

Fig. 4 Generated data model and testing. a) A true stimulus time series is generated and b) convolved with a transient shape to produce a signal. c) Gaussian noise is added, and d) ΔF/F0 filtering applied. e) The tested algorithm converts the signal into a time series (e.g., EWMA) and f) a threshold is applied to find predicted events. Finally, TPs, FPs and FNs, are converted to a F1 score to assess the event detector's accuracy.

The transient signal (Fig. 4b) was created by convolving unity with the transient shape defined in (6), with a relative amplitude of A = 600.

White noise (μ = 400, σ = 100) was added (Fig. 4c), to emulate realistic fluorescence data. The simulated, raw calcium intensities were converted as described in Section II.C, first with $\Delta F/F_0$ applied [18] (Fig. 4d) then provided to each algorithm to produce its statistic y_i, (Fig. 4e) which is finally has a threshold applied to result in predicted events (Fig. 4f).

Our goal is to identify transient events - such as that shown in Fig. 3 - that are evoked using controlled visual stimulus. Thus, predicted events occurring within 200 ms of the beginning of the simulated stimulus are considered true positives (TP). Events detected after 200 ms of the beginning of the simulated stimulus are considered FPs, as are events detected for a stimulus that already has one associated TP. A FN is defined by any window around a true event in which the algorithm did not detect anything. The accuracy of the event detectors was evaluated using the F1 score (7). The F1 assigns scores in a range from 0 to 1 [27] indicating no correct predictions to all correct predictions respectively:

$$F_1 = \frac{2TP}{2TP + FP + FN} \quad (7)$$

E. *Online event detector validation*

To validate the event detection system, we use the AOD random-access MPLSM (Fig. 5) for comprehensive imaging of sensory-evoked calcium activity in a visual stimulus processing neuron in the brain of the awake albino *Xenopus laevis* tadpole. This model animal was selected due to its transparency, which allows direct imaging of brain neurons in awake and immobilized specimens. Moreover, the external development of tadpoles permits imaging of early vertebrate brain developmental [28], [29].

The event detectors were tested using the same dataset from online experimentation. *Xenopus laevis* tadpoles were mounted into a custom, laser projection, visual stimulation chamber for analysis in our AOD random-access MPLSM. The experimental routine for system validation, was used to

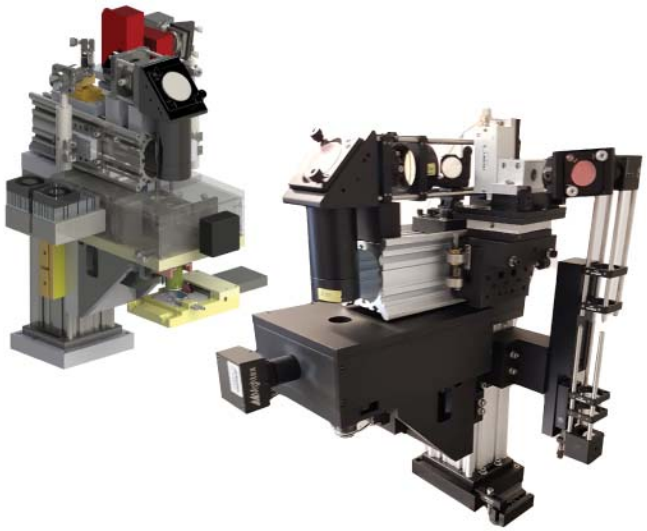

Fig. 5 The random-access, acousto-optic, MPLSM. (top-left) CAD design of the microscope and (bottom-right) implemented system used in this work.

identify a neuron's dendritic arbor morphology and observe the functional activity in response to a controlled, visual stimuli paradigm - presenting 8 stimuli: 4 light-off (OFF) and 4 light-on (ON) on opposing background over 68 s.

The tadpoles were scanned using a 'rapid-scan', 3D-grid-array search with a grid spacing of approximately 8.5 μm in order to locate neurons in the region of the optic-tectum (i.e. visual processing region). Active regions in the brain were identified by observing the output of the event detectors in the POI traces and change was identified and indicated to the operator after approximately 60 seconds of scanning. Tadpoles displaying activity were imaged with a 3D X-Y image stack of the tectal region at 1.5 μm spacing. An operator 'traced' the neuron on the X-Y image stack creating an interpolated 3D representation of the user-traced neuron with POIs at < 2.5 μm intervals over the dendritic arbor. The POI image coordinates were converted to world coordinates and rapidly imaged using the RAM MPLSM system.

F. Xenopus laevis preparation

Freely swimming albino *Xenopus laevis* tadpoles were reared and maintained in 10% Steinberg's solution [30]. In order to transfect brain neurons for expression of calcium sensors we used electroporation of plasmid DNA. Seven days post-fertilization, tadpoles were anesthetized using 0.01 % solution of MS-222 (A5040-25G, Sigma-Aldrich) for 5 min. A handheld pressure injector, connected to a micropipette holder (MEH7W15, WPI), loaded the tectum by pressure injection. A borosilicate micropipette (BF150-75-10, Sutter Inc.) pulled on a micropipette puller (P-97, Sutter Inc.) was filled deliver the solution containing 2 $\mu g/\mu L$ plasmid DNA, GCaMP6m in calcium-free, Ringer's solution (in mM: 116 NaCl, 1.2 KCl, 2.7 $NaHCO_3$). The tadpole brains were then exposed to trains of voltage pulses to induce electroporative transfection. Prior to experimentation, tadpoles were paralyzed in a bath using 2 mM pancuronium dibromide (0693/50, Tocris) for 5 minutes. All experimental procedures were conducted on Stg. 49 tadpoles according to the guidelines of the CCAC and were approved by the Animal Care Committee of the University of British Columbia's Faculty of Medicine.

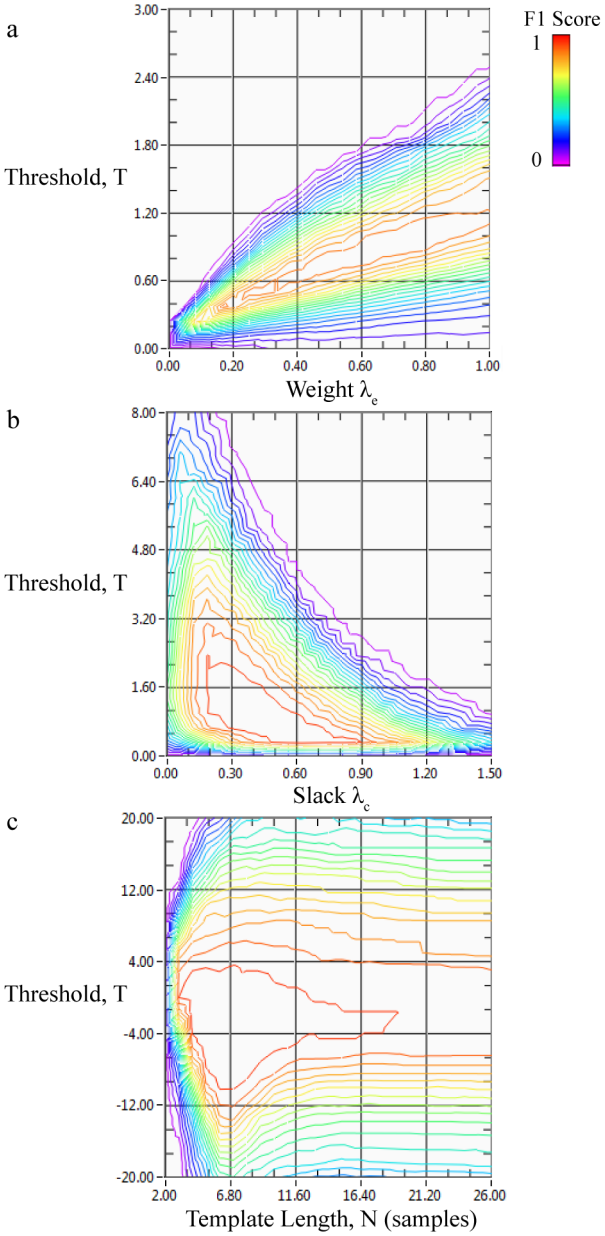

Fig. 6 F1 score performance evaluation contour maps. (a) EWMA heat map, showing a narrow band of optimal results, with weight λ_e ranging from 0 to 1. Maximum F1 score is 0.92. (b) cusum heat map, with a large central area of ideal performance F1=1. (c) MF heat map, showing a range of viable thresholds for F1=1, centered around T=0.

III. Results and Discussion

A. Event detector offline data validation

The performance of the three event detectors was evaluated by comparing the F1 scores (7) and subroutine execution time of each event detector over 5 million trials (25 parameter values x 25 threshold values x 100 stimuli x 8 seconds x 10hz). The performance results and computational efficiencies of each event detector are visually summarized in the contour maps in Fig. 6(a-c) and in Table I respectively. Parameter-pair values encapsulated in red contours indicate

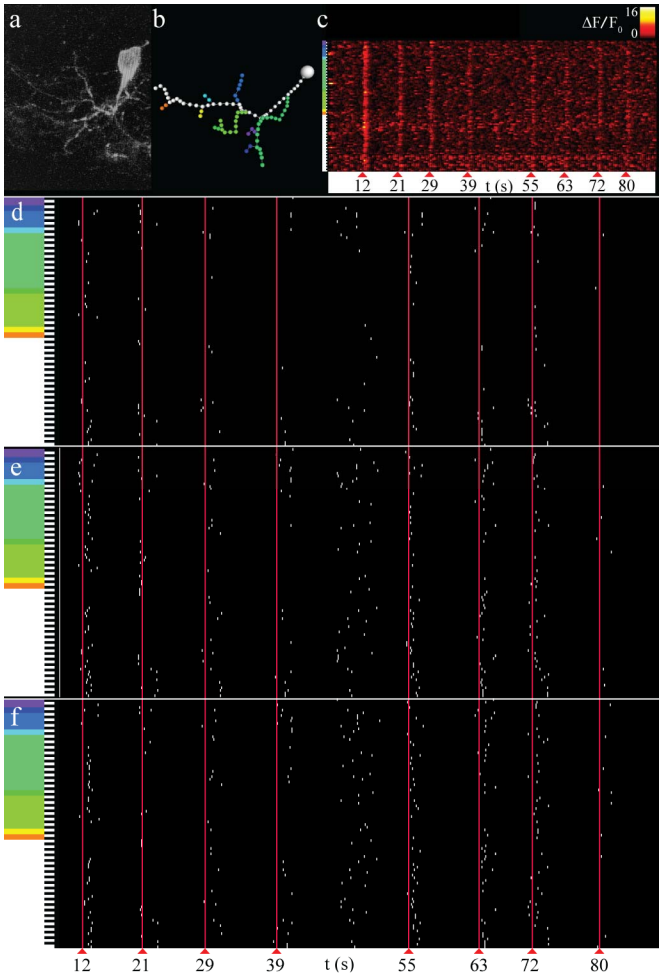

Fig. 5 Online event detection tests. (a) A neuron scanned using the RAM MPLSM and the (b) skeletonized 3D neuron following the user tracing X-Y images. (c) The output trace, $\Delta F/F_0$, of each POI containing the input, x_i, to the 3 event detectors. More significant activity (i.e. brighter regions on the traces, can be seen where the stimuli are presented. (d-e) EWMA, cusum and the MF respectively. Each event detector inputs the data from *c* and attempts to identify transients for each stimulus presented (the red vertical line).

regions where pairs have scored a higher F1 score (i.e. detection of more TPs). Parameter-pair values extending from the red contour to the violet contour indicate an increasingly lower F1 score (i.e. detection of fewer TPs/more FPs, FNs). Contour maps displaying a wide range of parameter choices (i.e. X-axis) that intersect with thresholds (i.e. Y-axis) within the red contour are more accurate event detectors and have a higher versatility with-respect-to event detector operation.

The EWMA is a simple, event detector to implement and is efficient to calculate with only four mathematical operations. The threshold can be estimated easily using (3), which was validated in our trials, shown in the contour plot (Fig. 6a). The EWMA's weight parameter is more intuitive to set than the other two event detectors; however, the contour plot indicates a narrow range of λ_e for system stability.

The cusum, like the EWMA, is a fairly simple event detector to implement, though does require maintaining a signal average. The cusum is a less intuitive event, and in our experience, confusion exists when describing the meaning of the slack variable λ_S. In the contour plot in Fig. 6b, we observed the relationship between λ_S and a suitable threshold:

TABLE I. EVENT DETECTION COMPUTATIONAL EFFICIENCY

	EWMA	cusum	MF
# parameters	1	1	4
# Mathematical operations	4	7	Template length
Exec. time / sample (Mean, µs)	0.30	0.47	6.4
Exec. time / sample (Std. Dev., µs)	7.7×10^{-6}	7.9×10^{-6}	250×10^{-6}

TABLE II. PARAMETER CHANGE RESULTS SUMMARY

	EWMA	cusum	MF
Parameter value	***Weight λe***	***Slack, λc***	***Template length, N***
Increase	Higher recall	Higher precision	Higher F_1 accuracy
Decrease	Higher precision	Higher recall	Faster

TABLE III. PARAMETER RANGES FOR EVENT DETECTOR

	EWMA	cusum	MF
Parameter	λ_e	λ_c	*N*
Param. range	0 - 1	0 - 1.5	2 - 24 samples (0.2 - 2.4 s)
Sugg param.	0.1 - 0.3	0.1 - 0.5	>= 12
Thrsh. Range	0 - 3	0 - 8	-20 - 20
Sugg Thrsh.	Eq. (3)	Eq. (8)	0

TABLE IV. ONLINE EVENT DETECTOR SUMMARY

	ON Stimulus #				OFF Stimulus #			
	Events before	***Events after***	***mean (samps)***	***StDev. (samps)***	***Events before***	***Events after***	***Mean (samps)***	***StDev. (samps)***
EWMA	23	42	8.0	4.4	11	55	6.0	4.6
cusum	32	86	8.4	4.4	12	109	6.0	4.4
MF	15	86	8.8	4.1	14	117	7.17	4.1

$$T = 1/2\lambda_s \quad (8)$$

The cusum, similar to the EWMA also has a wide range of λ_s selections to adjust the rate at which the threshold is reached.

The MF is a more complex event detector to implement and comprehend in comparison with the other event detectors. The MF requires many more parameters than the other detectors, *a priori* knowledge of signal shape, and is the slowest to calculate. In our offline experimental trials, the execution time of the MF was in the order of 10 times slower than both the EWMA and the cusum (Table I). The MF also requires at least *N* values to store and update each sample. Provided *N* remains small, this is still feasible to perform in real-time. As seen in Fig. 6c, the *MF* was less sensitive to changes in parameter (*N*) and has a stable threshold at *T*=0; however, increases in template size (*N*) results in a linear increase in calculation time as the ratio is calculated over the last *N* samples. Table II provides some guidelines for adjusting the EWMA, cusum, and MF parameters. Table III provides the parameter ranges used during the offline experimentation, as well as ranges for suggested parameters.

B. Event detector validation using neuron feedback

We demonstrated the utility of our system and the three event detectors by testing each one with evoked responses from a *Xenopus laevis* tectal neuron. We compared the output of each detector using the same input data by determining which events occurred first with respect to the initiation of the visual stimulus for each POI (Table IV). In total, the system

monitored data from 94 POIs on a neuron that had 173 μm total branch length for a duration of 68 seconds. For the eight stimuli applied, the MF detected the most events that occurred following the start time of each stimulus (N_{ON} = 86, N_{OFF} = 117, i.e. number during the ON and OFF stimuli respectively). For each POI with an event detected following the stimulus, the EWMA (μ_{ON} = 8.0, σ_{ON} = 4.4, μ_{OFF} = 6.0 σ_{OFF} = 4.6), and cusum (μ_{ON} = 8.4, σ_{ON} = 4.4, μ_{OFF} = 6.0, σ_{OFF} = 4.4) reported events with similar latencies and before the MF, and the MF (μ_{ON} = 8.8 σ_{ON} = 4.1, μ_{OFF} = 7.2 σ_{OFF} = 4.1) took the greatest number of samples to respond.

IV. CONCLUSION

We have designed a system that is capable of rapidly scanning and automatically detecting visually stimulated evoked events in brain neurons in an *in vivo* model in real-time using a random-access MPLSM. Our event detection system will assist the neuroscience community in understanding how neurons integrate and process synaptic inputs in the visual system and potentially, in other modalities that are used for characterizing fluorescence-based calcium activity in real-time.

We evaluated the performance (i.e. F1 score) and measured the computational timing characteristics of the EWMA, cusum and the MF. Furthermore, we tested each event detector using the calcium intensity output from a neuron inside an awake, and intact brain in *Xenopus laevis*. Our analysis of the generated data provided a controlled means of evaluating the three event detectors. The MF's event detection accuracy provided the best performance with-respect-to accuracy and sensitivity to changes in operator-set parameters. Nevertheless, the MF consumes the most computational time, is less intuitive to use and requires a greater number of parameters for the operator to comprehend. Furthermore, the MF requires the operator to create a 'template-signal' to detect. The cusum and EWMA have similar accuracy performance and similar sensitivity to parameter changes. Both the cusum and EWMA have low computational requirements and performed in one-tenth of the time taken by the MF making these event detectors much more desirable to implement when analyzing an extremely large number of POIs. Finally, both the EWMA and the cusum are more versatile since they do not require shape parameters, similar to the MF, or an extensive knowledge of the calcium transient.

REFERENCES

[1] T. Rose, P. M. Goltstein, R. Portugues, and O. Griesbeck, "Putting a finishing touch on GECIs," *Front. Mol. Neurosci.*, vol. 7, Nov. 2014.

[2] J. Nakai, M. Ohkura, and K. Imoto, "A high signal-to-noise Ca2+ probe composed of a single green fluorescent protein," *Nat. Biotechnol.*, vol. 19, no. 2, p. 137, Feb. 2001.

[3] T. Chen *et al.*, "Ultrasensitive fluorescent proteins for imaging neuronal activity," *Nature*, vol. 499, no. 7458, pp. 295–300, Jul. 2013.

[4] B. L. Sabatini, T. G. Oertner, and K. Svoboda, "The life cycle of ca(2+) ions in dendritic spines," *Neuron*, vol. 33, pp. 439–453, Jan. 2002.

[5] A. Bullen and P. Saggau, "High-speed, random-access fluorescence microscopy: I. High-resolution optical recordings with voltage-sensitive dyes and ion indicators," *Biophys. J.*, vol. 73, pp. 477–491, Jul. 1997.

[6] G. Katona *et al.*, "Fast two-photon in vivo imaging with three-dimensional random-access scanning in large tissue volumes," *Nat. Methods*, vol. 9, no. 2, pp. 201–208, Jan. 2012.

[7] R. Salomé *et al.*, "Ultrafast random-access scanning in two-photon microscopy using acousto-optic deflectors," *J. Neurosci. Methods*, vol. 154, no. 1–2, pp. 161–174, Jun. 2006.

[8] K. D. R. Sakaki, K. Podgorski, and K. Haas, "Comprehensive, in vivo and awake imaging of brain neural activity using an actor framework-based, random-access, two-photon laser-scanning microscope system," *IEEE Trans Biomed Eng*, vol. Submitted, Jan. 2018.

[9] N. Friedman, A. Kaplan, and N. Davidson, "Acousto-optic scanning system with very fast nonlinear scans," *Opt. Lett.*, vol. 25, no. 24, pp. 1762–1764, 2000.

[10] L. Redmond and A. Ghosh, "Regulation of dendritic development by calcium signaling," *Cell Calcium*, vol. 37, no. 5, pp. 411–416, May 2005.

[11] M. W. Cowan, T. C. Südhof, and C. F. Stevens, *Synapses*. Baltimore: Johns Hopkins University Press, 2001.

[12] N. Burnashev, H. Monyer, P. H. Seeburg, and B. Sakmann, "Divalent ion permeability of AMPA receptor channels is dominated by the edited form of a signal subunit," *Neuron*, vol. 8, pp. 189–198, Jan. 1992.

[13] D. E. Clapham, "Calcium Signaling," *Cell*, vol. 131, no. 6, pp. 1047–1058, Dec. 2007.

[14] F. Helmchen, K. Imoto, and B. Sakmann, "Ca2+ buffering and action potential-evoked Ca2+ signaling in dendrites of pyramidal neurons," *Biophys. J.*, vol. 70, no. 2, pp. 1069–1081, Feb. 1996.

[15] G. Katona *et al.*, "Roller Coaster Scanning reveals spontaneous triggering of dendritic spikes in CA1 interneurons," *Proc. Natl. Acad. Sci.*, vol. 108, no. 5, pp. 2148–2153, Feb. 2011.

[16] X. R. Sun *et al.*, "Fast GCaMPs for improved tracking of neuronal activity," *Nat. Commun.*, vol. 4, Jul. 2013.

[17] J. Waters, A. Schaefer, and B. Sakmann, "Backpropagating action potentials in neurones: measurement, mechanisms and potential functions," *Prog. Biophys. Mol. Biol.*, vol. 87, no. 1, pp. 145–170, Jan. 2005.

[18] H. Jia, N. L. Rochefort, X. Chen, and A. Konnerth, "In vivo two-photon imaging of sensory-evoked dendritic calcium signals in cortical neurons," *Nat. Protoc.*, vol. 6, no. 1, pp. 28–35, Jan. 2011.

[19] J. O. Westgard, T. Groth, T. Aronsson, and C. H. De Verdier, "Combined Shewhart-cusum control chart for improved quality control in clinical chemistry.," *Clin. Chem.*, vol. 23, no. 10, pp. 1881–1887, Oct. 1977.

[20] M. Basseville and I. V. Nikiforov, *Detection of abrupt change theory and applications*. Englewood Cliffs, NJ: Prentice-Hall, 1993.

[21] D. C. Montgomery, *Introduction to Statistical Quality Control*, 4th ed. New York: Wiley, 2001.

[22] F. Gustafsson, *Adaptive Filtering and Change Detection*. Chichester: Wiley, 2001.

[23] K. Sakaki, H. Esmaeilsabzali, N. Dechev, R. D. Burke, and E. J. Park, "A generalized tip-membrane contact detection algorithm for automated single cell electroporation using statistical process control," *IEEE Trans. Autom. Sci. Eng.*, vol. 9, no. 2, pp. 226–236, Apr. 2012.

[24] J. N. Kerr, D. Greenberg, and F. Helmchen, "Imaging input and output of neocortical networks in vivo," *Proc. Natl. Acad. Sci. U. S. A.*, vol. 102, no. 39, pp. 14063–14068, 2005.

[25] A. F. Szymanska, C. Kobayashi, H. Norimoto, T. Ishikawa, Y. Ikegaya, and Z. Nenadic, "Accurate detection of low signal-to-noise ratio neuronal calcium transient waves using a matched filter," *J. Neurosci. Methods*, vol. 259, pp. 1–12, Feb. 2016.

[26] T. Deneux *et al.*, "Accurate spike estimation from noisy calcium signals for ultrafast three-dimensional imaging of large neuronal populations in vivo," *Nat. Commun.*, vol. 7, Jul. 2016.

[27] D. M. Powers, "Evaluation: from precision, recall and F-measure to ROC, informedness, markedness and correlation," *J. Mach. Learn. Technol.*, vol. 2, no. 1, pp. 37–63, Feb. 2011.

[28] K. Haas, K. Jensen, W. C. Sin, L. Foa, and H. T. Cline, "Targeted electroporation in Xenopus tadpoles in vivo – from single cells to the entire brain," *Differentiation*, vol. 70, no. 4–5, pp. 148–154, Jun. 2002.

[29] E. S. Ruthazer and C. D. Aizenman, "Learning to see: patterned visual activity and the development of visual function," *Trends Neurosci.*, vol. 33, no. 4, pp. 183–192, Apr. 2010.

[30] D. Dunfield and K. Haas, "Metaplasticity governs natural experience-driven plasticity of nascent embryonic brain circuits," *Neuron*, vol. 64, no. 2, pp. 240–250, Oct. 2009.